energies

MDPI

Article

Modeling and Performance Analysis of a Solar Pond Integrated with an Absorption Cooling System

Ahmad Saleh

Department of Mechanical Engineering, Zarqa University, Zarqa 13132, Jordan; abuhussein@zu.edu.jo

Abstract: Solar ponds are characterized by high storage capacity and the ability to provide a stable and continuous power source. Careful selection of the extraction rate helps to maintain supply temperature in a range suitable for the operation of an absorption unit. This study proposed a system in which a solar pond is coupled with an absorption chiller to investigate the resulting advantages. The chiller is cooled by using water of the upper convective zone, which ensures that the limit of deterioration of its performance is not reached and eliminates the need for an expensive cooling system. The key parameters in terms of ambient temperature, solar radiation, pond specifications, and cooling and refrigeration temperatures are investigated to optimize the proposed system design. The prediction of the model showed good agreement with the experimental results. By choosing the appropriate place to implement the system, such as the Dead Sea area, which enjoys favorable climatic conditions, it was found that a pond with an area of 3000 m^2 can produce a heat rate at a temperature of 80 °C that can drive a chiller with 126.3 kW cooling capacity, with overall *COP* of 0.183. Based on this study, it appears that this type of system is feasible and suitable for cooling production, especially in hot regions.

Keywords: solar pond; efficiency of solar pond; extraction rate; absorption chiller; coefficient of performance; cooling capacity

check for updates

Citation: Saleh, A. Modeling and Performance Analysis of a Solar Pond Integrated with an Absorption Cooling System. *Energies* **2022**, *15*, 8327. https://doi.org/10.3390/en15228327

Academic Editor: Surender Reddy Salkuti

Received: 15 October 2022
Accepted: 2 November 2022
Published: 8 November 2022

Publisher's Note: MDPI stays neutral with regard to jurisdictional claims in published maps and institutional affiliations.

Copyright: © 2022 by the author. Licensee MDPI, Basel, Switzerland. This article is an open access article distributed under the terms and conditions of the Creative Commons Attribution (CC BY) license (https://creativecommons.org/licenses/by/4.0/).

1. Introduction

Reducing energy costs and preserving the environment by reducing emissions from the combustion of fossil fuels has been a priority for researchers for a while. In developing countries, energy consumption increases with increasing economic development. A few decades ago, interest emerged in developing salinity gradient solar ponds (SGSP) which can provide a convenient and less costly option to store heat at different seasonal cycles. They are also characterized by long-term storage capacity [1] that can be used to provide a continuous power source. This feature is of special importance when the load requires a stable and continuous power supply. In general, SGSP requires large amounts of cheap land, a good annual solar radiation average, a fresh water source, and large amounts of salt. Many places in the world meet these requirements, which makes them suitable for setting up solar pond systems.

Amigo et al. [2] showed that when the water table below the pond is deep, the ground acts as an additional heat storage volume, permitting more stable temperatures in the pond throughout the year and making it more suitable for the constant heat demand. Several researchers have focused their attention on the possible applications of energy stored in solar ponds. A review of the literature revealed that solar ponds were proposed as a power source for a large number of applications including power generation, salt production, process heating, desalination, and space heating and cooling. Saleh et al. [3] conducted a comprehensive analysis of a solar pond coupled with a desalination plant and showed that a 3000 m^2 surface area solar pond installed near the Dead Sea can provide an annual average production rate of 4.3 L/min distilled water.

Various analytical and numerical models were presented to investigate the performance of solar ponds. Analytical models usually require some simplifying assumptions to reach a reasonable estimate for performance. Weinberger [4] presented a model using the superposition technique and assumed an upper convective zone (*UCZ*) of negligible thickness and pond surface temperature equal to the ambient temperature. It was found that at a given extraction temperature, there is a specific depth at which the available heat extraction rate is at its highest. Rabl et al. [5] presented a model to estimate annual average variation in pond temperature neglecting the thickness of the *UCZ* and found that for a given location, load, and average extraction temperature, there is an optimum non-convective zone (*NCZ*) thickness that corresponds to a minimum pond area. Kooi [6] presented a model with a better estimate of performance assuming a *UCZ* with finite thickness and considering that the pond was operating in steady-state conditions and giving annual average time-independent solutions. Verma et al. [7] presented an analytical solution for evaluating the performance of solar ponds assisted by heat recovery from the ground beneath considering the conditions that can actually be achieved. It was found that the effectiveness of heat extraction from the ground has significant effects on various aspects of solar pond performance, such as stability, entropy production, and optimum *NCZ* thickness.

Numerical methods have the advantage of giving more freedom in which appropriate initial and boundary conditions are combined and provide a more realistic representation of climatic conditions, as well as load differences. Hawlader et al. [8] presented a model and found that as the thickness of the *NCZ* increases from 0.5 to 2.3 m, the maximum temperature initially increases and then tends to decrease due to the increased insulation effect of solar radiation with depth. It seems that the optimal values for the depth of the *NCZ* range are from 1–1.5 m. Tian et al. [9] proposed an active method of using an external magnetic field to repress the intense convection region of the solar pond and improve its stability. It was found that when magnetic control is exerted on a solar pond, the decrease in the *NCZ* thickness caused by interface erosion changed from 14.75% to 0. A numerical study of heat and mass transfer and stability in solar ponds by using CFD in a transient regime was presented by [10]. It was revealed that the buoyancy ratio is important in reducing the temperature of the *UCZ* and in maintaining the temperature of the lower convective zone (*LCZ*). A CFD simulation set-up was developed by [11] to obtain a fully versatile model applicable to any practical scenario by which it was possible to accurately evaluate the heat loss to the surroundings, the irradiance absorbed by the solar pond, and the thermal performance of the pond throughout the year.

Many experimental investigations were also implemented in different regions of the world. Perhaps one of the first and most important is the El Paso solar pond, a demonstration project operated by the University of Texas at El Paso. The pond has a surface area of 3000 m^2 and a depth of 3.2 m and operates in a temperature range of 77–87 °C [12]. It was used to deliver industrial process heat, generate electric power, and power water desalting facilities. The range of operation and stability of the supply temperature of solar ponds, based on the findings of many researchers, can provide a suitable source for the operation of absorption chillers. Such a source allows the systems to run for long periods without being affected by fluctuations in solar radiation. A comparison of the performance of solar ponds with flat plate collectors showed that solar ponds are more effective at higher temperatures with built-in heat storage at a substantially lower cost [13]. The limited performance of flat plate collectors and the cost of more advanced designs of collectors such as an evacuated tube or low-concentration systems established the tendency to adopt solar ponds as large-scale collectors for large cooling applications using currently available conventional absorption chillers.

Absorption chillers are environmentally friendly and require low-grade heat sources to operate, thus providing lower power supply costs than electrical energy [14]. The chillers using the absorbent–refrigerant pair LiBr–H_2O are suitable for solar applications as they

are simple in design and operation, cheap in cost, have high *COP*, and operate at low generator temperatures.

Many researchers investigated LiBr–H_2O systems presenting theoretical and experimental studies. Fathi et al. [15] presented a simulation model of a single-effect LiBr–H_2O absorption machine. The *COP* was estimated in the function of generator and evaporator temperatures. The results showed that there is a temperature limit at which the system does not work if it exceeds it down or up. An investigation conducted to improve the operation of solar absorption systems in hot regions was presented by Saleh et al. [16]. It was found that the best system performance takes place at generator temperatures between 75 and 80 °C. With a proper selection of component temperatures, the *COP* of the system can exceed a value of 0.8. A novel model was developed by Ren et al. [17] for the analysis of absorption refrigeration systems and comparison between LiCl–H_2O and LiBr–H_2O systems. The results indicated that LiCl–H_2O systems have higher *COP* and utilization efficiency, especially in the case of a lower generator or higher condenser temperatures, but their operation is more restricted due to crystallization. Different types of absorption systems (specifically, single, double, triple, and quadruple effect absorption cycles) were investigated when powered by an evacuated tube collector and using hybrid nanofluids as a heat transfer fluid [18]. The results revealed that using hybrid nanofluids leads to a higher collector efficiency compared to other types of fluids. Saleh et al. [19] investigated the enhancement of vacuum wastewater treatment plant operation using solar absorption systems. It was found that by using the heat provided by the absorption system supplied at low-temperature levels, the evaporation rate in the vacuum treatment plant exceeded 60 kg/h. A comparison between two different types of collectors, parabolic trough and evacuated tube, driving water–lithium bromide absorption systems to select the best-operating conditions was presented by [20]. The results revealed that a parabolic trough collector combined with H_2O–LiBr gives lower design aspects and minimum rates of hourly costs. The coefficient of performance was in the range of 0.5–0.9.

Most of the countries in the Middle East are developing countries and their energy requirements are reaching high levels that exceed those of many industrialized countries. However, these countries enjoy plenty of solar radiation, a lot of sunny days, and uninterrupted sunlight that may reach 3000 h per year. Vast areas of these countries receive annual average daily global irradiance between 6 and 7 kWh/m^2 and solar intensity exceeding 1000 W/m^2 [21]. On the other hand, the importance of cooling to improve health and living standards, especially in hot regions, is evident in many applications such as refrigeration, sterilization, and food preservation. There are many cases where there is a need for refrigeration 24 h a day, such as air conditioning needs, especially in hot countries. This makes solar ponds, especially those with long-term storage capacity, clearly preferable over solar collector systems, which are not suitable for providing power at times in the absence of the sun. Even if the collection system was designed to provide heat for 24 h, it would require a large, impractical storage tank system.

Tsilingiris [22] presented a numerical analysis that allows the investigation of solar pond design to be coupled with a commercially available absorption chiller. The results are useful for rough design and pond size selection for the operation of a chiller directly from solar ponds. Later, he investigated the possibility of using solar ponds as low-cost solar collectors combined with commercial absorption chillers in large-scale solar cooling design [23]. The numerical solution of the nonlinear equations involved provided results that relate chiller capacity with pond design and environmental parameters. An SGSP was suggested by [24] as a collector to drive an absorption chiller used to cool air for a house using the weather data for Baghdad in Iraq. The results showed that a solar pond area of 400 m^2 can provide cooling for a house with a floor area of 125 m^2. Salata et al. [25] proposed the application of solar energy stored in solar ponds for conditioning small buildings, through the use of absorption chillers. A feasibility analysis was performed in some places with a suitable climate to make the proposed solution sustainable in terms of energy utilization.

By reviewing the available literature in this field, it can be seen that many researchers have extensively studied solar ponds with their various applications and others have extensively studied absorption systems operating with different sources. Little efforts have been made to investigate their combination and evaluate the consequent benefits. This is a gap that deserves to be explored. The characteristics of the solar ponds with their high storage capacity, supply temperature stability and compatibility with the operating conditions of absorption chillers make them a preferred choice to drive absorption cooling systems. This coupling helps to avoid known difficulties in using solar energy, its low density and irregularity.

In this study, an absorption chiller integrated with a salinity gradient solar pond is proposed, modeled, and investigated. A computer code was developed and implemented through the software MATLAB/2016b. The operation of the system is investigated in different climatic conditions analyzing the influence of different parameters that affect the performance of the system. The system was optimized to operate in the Dead Sea area in Jordan, distinguished by high solar density, high ambient temperature, and availability of saline water. In such areas, it is expected that salinity gradient solar ponds will be able to withstand a full load of large-scale cooling plants without relying on auxiliary sources. However, the results can be generalized to many countries with different climatic conditions. The main objective behind this was to evaluate the feasibility of coupling absorption systems with solar ponds and to demonstrate the resulting advantages.

2. Methodology

A schematic of the proposed system is shown in Figure 1. The solar pond consists of three layers. The upper convective zone has a temperature close to ambient temperature and low salt content. The lower convective zone is salty and constitutes the storage place for energy. The significant middle gradient region or the non-convective zone separates the other two regions. The *NCZ* acts as a transparent insulator so that sunlight will be trapped in the storage *LCZ*, from which useful power is drawn. This can be explained by noticing that the salt gradient increases the density of the brine with depth and then nullifies the buoyancy effect of the warm water below, which would otherwise lose its heat as it rises to the surface. To maintain the salt concentration gradient, fresh water should be added to the *UCZ* and concentrated brine should be added to the *LCZ* from time to time.

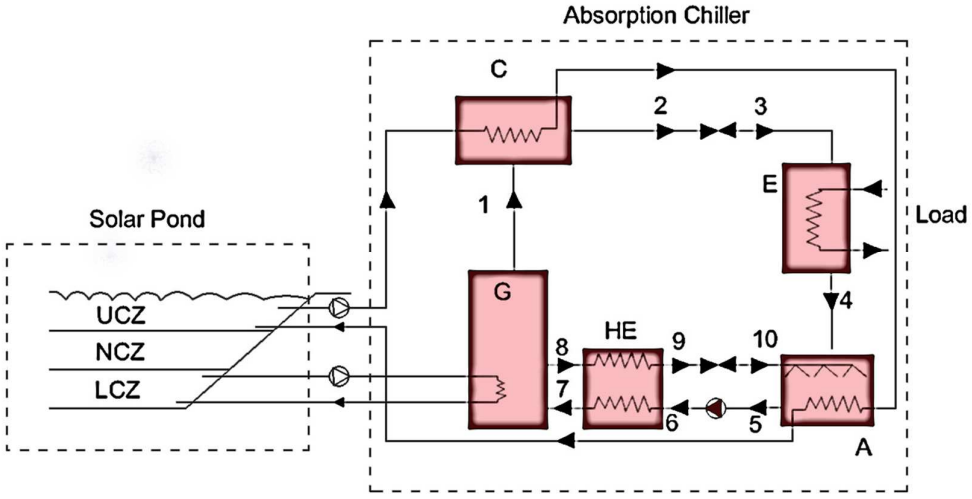

Figure 1. A schematic of the system: a solar pond coupled with an absorption chiller for cooling applications. A: Absorber, C: Condenser, E: Evaporator, G: Generator, HE: solution heat exchanger.

The thickness of the *LCZ* is usually recommended to be 0.1 m [26]. This layer performs the function of protecting the *NCZ* from wind and rain. The thickness of this layer has two opposite effects. One is to increase the stability of the *NCZ* and the other is to reduce the transmission of solar radiation to the *LCZ*, which leads to a decrease in the temperature

of the *LCZ* and a decrease in the energy stored there. A drop of one degree is observed for each 0.1 m increase in the thickness of the layer. In the proposed system, this layer is used to cool the condenser and the absorber of the chiller, and therefore the thickness must be appropriate to counteract the effect of the cooling water recirculation flow. Based on this, a value of 0.4 m will be chosen as an intermediate value to balance the opposing effects.

The *NCZ* thickness is estimated with other parameters to optimize the performance of the system. The required concentration of the *LCZ* can be maintained by utilizing the high-concentration brine that, if it was extracted from a place rich in salt such as the Dead Sea, would reduce the cost significantly. Providing the necessary amount of salt is the most important factor in cost reduction. The low concentration at the *UCZ* is controlled by discharging the saline line in a suitable salty place.

An important way to improve the efficiency of a solar pond is to reduce heat losses from the bottom and sides of the pond. This fact has encouraged many researchers to focus on developing pond liners [27]. However, this issue needs further research in the future. Other efforts were exerted in developing thermal barrier coatings by ingot evaporation in electron-beam physical vapor deposition [28]. Although these efforts were dedicated to other applications, the characteristics of the liner produced such as the high insulation effect and the reduced thickness may draw attention to the use of this technology in the design of solar ponds.

Hot brine from the *LCZ* will be pumped out of the pond to transfer thermal power to the generator of the absorption chiller. Assuming heat losses in the pipe network connecting the pond and the chiller are to be ignored, hot water exchanges heat with the LiBr–H_2O solution and water vaporizes inside the generator at a temperature equal to that of *LCZ*. Additionally, the heat extraction rate from the pond will equal the heat supply rate to the generator. The boiled-off water vapor (point 1), leaving a strong solution of refrigerant in the generator, moves to the condenser where it is cooled and condensed (point 2) and then passes through the expansion valve (point 3) to the evaporator. In the evaporator, evaporation occurs (point 4) due to low pressure to provide the desired cooling effect. The strong solution that remained in the generator (point 8) passes through the heat exchanger (points 9–10) to the absorber where it absorbs the water vapor leaving the evaporator to become a weak solution (points 5–6). Passing through the heat exchanger (point 7), the hot strong solution exchanges heat with the cold weak solution moving to the generator from the absorber.

Water pumped out from the *UCZ* will be used to cool both the condenser and the absorber. Rejected heat is then dissipated mainly by evaporation from the surface of the pond, the effectiveness of which is significantly affected by the prevailing wind speed, ambient temperature, and relative humidity. This concept appears to be attractive as it eliminates the need for use of an expensive cooling tower.

For efficient operation of the chiller, maximum values of the generator and evaporator temperatures and minimum values of the condenser and absorber temperatures should be maintained.

The pressure reduction in the condenser due to low cooling water temperature below a certain value should be avoided to avoid crystallization that occurs when the hot solution rich in LiBr salt is cooled in the solution heat exchanger to low temperatures. Solid crystal formation can block pipes and valves.

The control strategy can be achieved based on the inputs and outputs of the system. The control system often necessitates sensing a plurality of conditions of operation of the system. The lack of study and research for this type of system has led to a lack of information related to the appropriate control systems. Before the chiller can be started, the solar pond has to be warmed up until the temperature of *LCZ* exceeds the start-up temperature of the chiller. The condenser and absorber cooling water temperature cannot be controlled because it depends on the temperature of the *UCZ* which depends on the ambient conditions. In addition to that, the *UCZ* temperature when increased has two

opposing effects, one is to improve the performance of the chiller and the second is to lower the efficiency of the pond so that the impact on the overall system performance is reduced.

If the cooling load drops down or the hot water temperature exceeds the level needed, the chilled water temperature can be controlled by mixing the hot water return flow with the hot supply flow via a three-way valve to achieve the necessary temperature level. If the hot source temperature is lower than needed, the extraction rate can be reduced to keep it at the reference value required. If the hot source temperature falls below the minimum driving temperature of the chiller, the generator pump is switched off and the chiller can only be started again after reaching the minimum required temperature. In this case, an installation of a backup system is necessary. To design a system capable of handling the entire cooling load, worst-case conditions must be taken into account, which makes the system oversized. However, due to the stability of the *LCZ* temperature and the high thermal capacity of the pond, it is expected that the oversizing will be limited.

The present level of technology allows the chillers to be commercialized either with high performance and capacities up to 12,000 kW or units with significantly small capacities of up to 2.5 kW [29] for small applications. This wide range of commercially available chillers allows easy selection of the rated capacity that suits the extraction rates of coupled solar ponds.

3. Mathematical Modeling

System modeling will be performed by taking into consideration the models of both the solar pond and absorption chiller to form the model of the coupled overall system.

3.1. Solar Pond Subsystem

To estimate the performance of the solar pond, a set of differential equations must be solved. To solve the differential equation for each zone, the matching conditions must be used in the separating surfaces between the zones and the boundary conditions on the upper and lower surfaces of the pond should be taken into account. Several simplifications are often made and are helpful to obtain reasonably good estimates of pond performance. In this study, the model proposed by Kooi will be adopted [6]. This model treats the solar pond as a steady-state system and presents time-independent solutions in the form of annual average values. The model assumes a finite thickness of the *UCZ* and thus gives a better estimate of performance with respect to models that assume the *UCZ* has a negligible thickness.

Zone boundaries are assumed to be stable and adjusted to maximum efficiency and heat extraction does not affect stability. The *UCZ* is assumed to have a constant temperature equal to the ambient temperature and to have low and uniform salinity. The *LCZ* is assumed to be at constant temperature and high uniform salinity. The bottom surface is assumed to be a blackbody to maximize the radiation absorption. It is supposed that the pond bottom and sides are insulated to avoid any heat losses. Therefore, the radiation energy reaching the *LCZ* is completely absorbed by the solution and the bottom of the pond. Edge effects due to absorption of insolation and heating of the walls are also assumed to be negligible. The thermal conductivity and optical properties of water are assumed to be independent of salinity and temperature and the depth is small compared to the lateral dimensions, therefore the temperature and salinity distributions change only vertically.

Although the model is simple and does not consider either temperature and density distribution in all directions or heat losses through the pond's bottom and sides, it is sufficient for the purpose. This can also be justified because the results obtained from many experimental and theoretical models showed that after a warming-up period, the pond retains a temperature almost stable and suitable for the absorption system operation over long periods if the extraction rate is controlled at a certain value. Considering the experimental results of the El Paso solar pond based on the years 1991–1993 [12], the variations in temperature during the summer season are less than 5 °C while the variation between day and night is about 1–3 °C. The theoretical analysis presented by Rabl et al. [5]

showed that the amplitude of variation decreases to zero as *NCZ* thickness increases to infinity. The inclusion of ground storage also contributes to increasing temperature stability. The theoretical model presented by Chakrabartya et al. [26] showed that after about 150 days of the warm-up period, the *LCZ* temperature is almost stabilized and fluctuates between 80 and 100 °C. At places with low latitudes, an almost constant steady state could be maintained throughout the year and the stabilization can be enhanced by adding reflectors.

The differential equation for the *NCZ* is given by:

$$k\frac{d^2T_{II}}{dx^2} = \frac{d\left(H_g\tau_r\tau_a\right)}{dx} = H_g\tau_r\frac{d\tau_a}{dx} \tag{1}$$

where:

k thermal conductivity of the fluid, $Wm^{-1}K^{-1}$;
T_{II} temperature of *NCZ*, °C;
x depth of water, m;
H_g annual average global solar radiation incident on the surface of the pond, Wm^{-2};
τ_r transmissivity based on reflection;
τ_a transmissivity based on absorption.

The values of τ_r and τ_a are estimated at the effective angle of incidence θ_1 given by:

$$cos\theta_1 = sin\varphi sin\delta + cos\varphi cos\delta cos\omega \tag{2}$$

The effective angle of incidence, θ_1, is estimated on the equinox day at 14:00.

The beam radiation transmissivity based on reflection is given by:

$$\tau_r = 1 - \rho_b \tag{3}$$

The beam radiation reflectivity ρ_b is evaluated as the average of the perpendicular and parallel components of unpolarized radiation [13]:

$$\rho_I = \frac{sin^2(\theta_2 - \theta_1)}{sin^2(\theta_2 + \theta_1)} \tag{4}$$

$$\rho_{II} = \frac{tan^2(\theta_2 - \theta_1)}{tan^2(\theta_2 + \theta_1)} \tag{5}$$

where θ_2 is the refraction angle that corresponds to the effective angle of incidence and is given by:

$$\frac{sin\theta_1}{sin\theta_2} = \frac{n_2}{n_2} \tag{6}$$

where n_1 and n_2 are refraction indices for the first and second mediums, respectively.

Integrating Equation (1) twice will yield:

$$kT_{II} = H_g\tau_r\int_{l_1}^{x}\tau_a dx + c_1x + c_2 \tag{7}$$

where c_1 and c_2 are integration constants. Considering the boundary conditions:

At $x = l_1$ $T_{II} = T_I$
At $x = l_2$ $T_{II} = T_{III}$

Solving for c_1 and c_2, the temperature distribution and the temperature gradient distribution expressions in the *NCZ* are:

$$k[T_{II}(x) - T_I] = H_g\tau_r\int_{l_1}^{x}\tau_a dx + \frac{(x - l_1)}{(l_2 - l_1)}\left\{k(T_{III} - T_I) - H_g\tau_r\int_{l_1}^{l_2}\tau_a dx\right\} \tag{8}$$

$$k\frac{dT_{II}}{dx} = H\tau_r\tau_a + [\frac{k(T_{III} - T_I) - H_g\tau_r\int_{l_1}^{l_2}\tau_a dx}{(l_2 - l_1)}] \quad (9)$$

The energy flow rate to *LCZ* at interface $x = l_2$ is:

$$A_p[H_g\tau_r(\tau_a)_{x=l_2} + \left\{-k\left(\frac{dT_{II}}{dx}\right)_{x=l_2}\right\}] \quad (10)$$

where A_p is the pond surface area.

Substituting Equation (8) with $x = l_2$ into Equation (9) and realizing that at a steady state, the energy flow rate at the interface $x = l_2$ into the *LCZ* is equal to the average annual heat extraction rate from the pond, gives:

$$Q_{load} = A_p[\left\{\frac{H_g\tau_r}{(l_2 - l_1)}\int_{l_1}^{l_2}\tau_a dx\right\} - \frac{k}{(l_2 - l_1)}(T_{III} - T_I)] \quad (11)$$

The annual average efficiency is obtained by dividing both sides of Equation (11) by $H_g A_p$ and is given by:

$$\eta = \left\{\frac{\tau_r}{(l_2 - l_1)}\int_{l_1}^{l_2}\tau_a dx\right\} - \frac{k}{(l_2 - l_1)}\left(\frac{T_{III} - T_I}{H_g}\right) \quad (12)$$

Using the equation of Rabl and Nielsen's for τ_a and replacing K'_j by K_j, gives [5]:

$$\int_{l_1}^{l_2}\tau_a dx = \sum_{j=1}^{4}\frac{A_j}{K'_j}\left(e^{K'_j l_1} - e^{K'_j l_2}\right) \quad (13)$$

where $K'_j = K_j/cos\theta_2$.

As for the constants A_j and K_j, they take the following values after fitting the experimental data available:

A_1 = 0.237, K_1 = 0.032 m^{-1} for 0.2 < λ > 0.6 μm
A_2 = 0.193, K_2 = 0.45 m^{-1} for 0.6 < λ > 0.75 μm
A_3 = 0.167, K_3 = 3 m^{-1} for 0.75 < λ > 0.9 μm
A_4 = 0.179, K_4 = 35 m^{-1} for 0.9 < λ > 1.2 μm

Thus, Equations (11) and (12) become:

$$Q_{load} = A_p[\left\{\frac{H_g\tau_r}{(l_2 - l_1)}\sum_{j=1}^{4}\frac{A_j}{K'_j}\left(e^{K'_j l_1} - e^{K'_j l_2}\right)\right\} - \frac{k}{(l_2 - l_1)}(T_{III} - T_I)] \quad (14)$$

$$\eta = \left\{\frac{\tau_r}{(l_2 - l_1)}\sum_{j=1}^{4}\frac{A_j}{K'_j}\left(e^{K'_j l_1} - e^{K'_j l_2}\right)\right\} - \frac{k}{(l_2 - l_1)}\left(\frac{T_{III} - T_I}{H_g}\right) \quad (15)$$

These equations are used to evaluate the pond's average annual performance or to estimate the area needed to achieve specific requirements.

Energy flows between the various zones of a typical salinity gradient solar pond are shown in Figure 2.

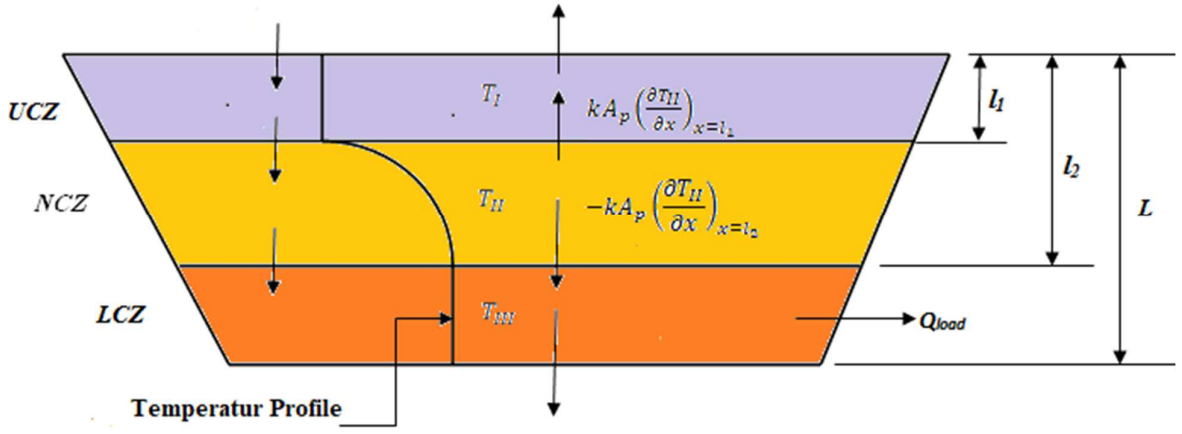

Figure 2. Energy flows of the various zones of a typical salinity gradient solar pond.

3.2. Absorption Subsystem

The lithium bromide water absorption chiller can run by a hot source at a temperature between 75 and 100 °C, which makes it suitable to be coupled with the solar pond as it has the same operating range.

The thermodynamic analysis is conducted with some assumptions [17]. Energy and mass balances of the system components form the basis of the model and are assumed to be in a steady state with homogenous variables within each component. The solution leaving the generator and absorber was assumed to be saturated in equilibrium at their pressure and temperature. The refrigerant flowing out of the condenser and evaporator is assumed also to be in a saturated phase. Heat losses and pressure drops in the components are neglected. In addition, the pump work is neglected. The simplifying assumptions adopted are thermally reasonable and widely verified in the extensive literature on absorption systems.

With reference to Figure 1, the mass and species balance equations in the generator and absorber are [16]:

$$\dot{m}_{ws} = \dot{m}_r + \dot{m}_{ss} \tag{16}$$

$$\dot{m}_{ws} x_{ws} = \dot{m}_{ss} x_{ss} \tag{17}$$

where the subscripts *ws*, *r*, and *ss* refer to the weak solution, refrigerant, and strong solution, respectively. The subscript *x* refers to the mass fraction of lithium bromide.

The rate of heat provided to the generator is:

$$\dot{Q}_g = \dot{m}_1 h_1 + \dot{m}_8 h_8 - \dot{m}_7 h_7 = \dot{m}_r h_1 + \dot{m}_{ss} h_8 - \dot{m}_{ws} h_7 \tag{18}$$

Referring to Equations (16) and (17), it is possible to determine the flow rates of strong and weak solutions as:

$$\dot{m}_{ws} = \frac{x_{ss}}{x_{ss} - x_{ws}} \dot{m}_r \tag{19}$$

$$\dot{m}_{ss} = \frac{x_{ws}}{x_{ss} - x_{ws}} \dot{m}_r \tag{20}$$

Based on generator and condenser temperatures, the concentration of the strong solution is given by:

$$x_{ss} = \frac{49.09 + 1.2T_g - T_c}{134.65 + 0.47T_g} \tag{21}$$

Similarly, by considering absorber and evaporator temperatures, the concentration of the weak solution is given by:

$$x_{ws} = \frac{49.09 + 1.2T_a - T_e}{134.65 + 0.47T_a} \tag{22}$$

For the solution heat exchanger, the energy balance is given by:

$$T_9 = \varepsilon_{HE} T_6 + (1 - \varepsilon_{HE}) T_8 \tag{23}$$

$$h_7 = h_6 + \frac{\dot{m}_8}{\dot{m}_6}(h_8 - h_9) = h_6 + \frac{\dot{m}_{ss}}{\dot{m}_{ws}}(h_8 - h_9) \tag{24}$$

The heat release rate due to cooling of the absorber is given by:

$$\dot{Q}_a = \dot{m}_4 h_4 + \dot{m}_{10} h_{10} - \dot{m}_5 h_5 = \dot{m}_r h_4 + \dot{m}_{ss} h_{10} - \dot{m}_{ws} h_5 \tag{25}$$

The heat release rate due to cooling of the condenser is given by:

$$\dot{Q}_c = \dot{m}_1 (h_1 - h_2) = \dot{m}_r (h_1 - h_2) \tag{26}$$

The cooling capacity which is equal to the rate of heat absorbed by the evaporator is given by:

$$\dot{Q}_e = \dot{m}_1 (h_4 - h_3) = \dot{m}_r (h_4 - h_3) \tag{27}$$

When pumping work is neglected, the coefficient of performance is given by:

$$COP = \frac{\dot{Q}_e}{\dot{Q}_g} \tag{28}$$

The enthalpy of water and water vapor at the outlets of the condenser, evaporator, and generator is given by [30]:

$$h = A + BT + CT^2 \tag{29}$$

where T corresponds to T_c at the outlet of the condenser; T_e at the outlet of the evaporator; and T_g at the outlet of the generator. A, B and C are constants.

The enthalpy of LiBr–H_2O solution passing through absorber and generator units is calculated in function of the solution temperature, T, and solution concentration, x (%), and is given by [31]:

$$h = \sum_0^4 A_n x^n + T \sum_0^4 B_n x^n + T^2 \sum_0^4 C_n x^n \tag{30}$$

where A, B and C are constant coefficients.

3.3. The Overall System

By coupling the solar pool with the absorption chiller, the overall system is established. Assuming negligible losses between the pond and the chiller, the extraction rate from the solar pond Q_{load} becomes equal to the rate of heat supplying the generator $\dot{Q}_g$ of the absorption system. Additionally, the temperature of the *LCZ* will be equal to the hot source temperature supplying the generator. Based on this, the coefficient of performance of the overall system becomes:

$$COP_{ov} = COP \times \eta \tag{31}$$

By substituting the variables

$$COP_{ov} = \frac{\dot{m}_r (h_4 - h_3)}{\dot{m}_r h_1 + \dot{m}_{ss} h_8 - \dot{m}_{ws} h_7} \times \left\{ \frac{\tau_r}{(l_2 - l_1)} \sum_{j=1}^{4} \frac{A_j}{K'_j} \left(e^{K'_j l_1} - e^{K'_j l_2} \right) \right\} - \frac{k}{(l_2 - l_1)} \left(\frac{T_{III} - T_I}{H_g} \right) \tag{32}$$

It is appropriate here to note that the variables involved in Equations (31) and (32) are interdependent. The *COP* of the absorption chiller is dependent on the absorber and condenser temperatures, which are dependent on the temperature of the *UCZ* (T_I). In addition, the *COP* depends on the temperature and on the rate of heat supply to the

generator, which are equal to the temperature of *LCZ* and to the heat extraction rate from the pond, respectively.

4. Results and Discussion

By running code after inserting input parameters such as climatic conditions, characteristics of the solar pond and characteristics of the absorption chiller, the performance parameters such as heat extraction rate from the pond, pond efficiency, hot source temperature flowing between the pond and the chiller, heat transfer rates to/from components of the chiller, cooling capacity and coefficients of performance of the chiller and of the overall system can be determined. It is assumed that the simulation results are considered when the system is operating at steady-state conditions after a warm-up period.

4.1. Solar Pond Subsystem

The surface area of the pond was selected to be 3000 m^2 for reasons of comparisons and validation with similar systems. By running the pond model to simulate the data introduced, the effects of various parameters were investigated.

4.1.1. Optimizing the *NCZ* Thickness with Respect to the Extraction Rate and Efficiency

Referring to the models used, the performance of the pond is affected mainly by the thickness of *NCZ*, the annual average global radiation and the annual average ambient temperature. On the other hand, the performance of the absorption chiller is affected by the temperature and the rate of heat supplied to the generator in addition to the temperatures of the other components.

Selecting three values for the hot brine temperature supplying the generator, 70, 80, and 90 °C, the thickness of the *NCZ* can be optimized as shown in Figure 3, and choosing an appropriate area to implement such a system effectively and economically, such as the Dead Sea in Jordan, where the annual average values of global radiation and ambient temperature are 5.52 kWh/m^2 and 24 °C, respectively [21,32]. It can be observed that at each temperature value, there is a value for the thickness of *NCZ* at which the performance is maximized. This result agrees with the result reported by Weinberger [4], who reported that at a given average extraction temperature, there is a certain depth of pond at which the rate of heat extraction is maximum. This can be explained by noting that the increase in *NCZ* thickness has two opposite effects, increasing insulation, which reduces the losses to the surrounding ambient, and reducing radiation penetrated to the *LCZ*, which reduces the power stored. If the value 80 °C is chosen as a reference temperature at which the chiller performs efficiently, as reported by many researchers, it can be observed that the available extraction rate increases rapidly with an *NCZ* thickness up to 1.5 m and then starts slowing down until it reaches its maximum value.

The extraction rate at a thickness of 1.5 is equal to 158.5 kW, while the maximum value is 168.4 kW at a thickness of 2.5 m. It can be concluded that a thickness of more than 1.5 m does not significantly improve performance and it will be more expensive to construct and maintain. Based on this, the value of 1.5 m will be chosen, where the resulting heat flow rate and efficiency, at a temperature of 80 °C, are 158.5 kW and 0.2297, respectively.

Another reason for this choice is to avoid the effects on long-term stability, zone interface erosion and boundary migration for a thickness of more than 1.5 m [33]. Therefore, the values corresponding to a thickness greater than 1.5 m are unrealistic and should not be taken into account as long as no measures are taken to ensure stability and prevent interface erosion of the *NCZ*.

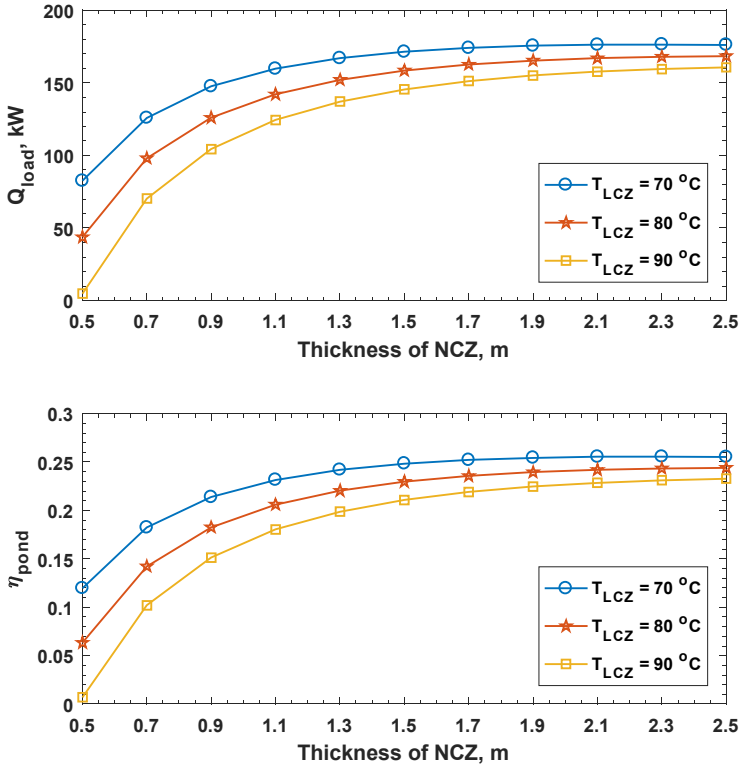

Figure 3. Effect of *NCZ* thickness and *LCZ* temperature on the performance of the pond.

4.1.2. Optimizing of the NCZ Thickness with Respect to the LCZ Temperature

The changes in the *LCZ* temperature with the thickness of *NCZ* are shown in Figure 4. It can be observed that for each extraction rate, the temperature of *LCZ* increases at a decreasing rate. This trend is consistent with the conclusion presented by Hawlader et al. [8].

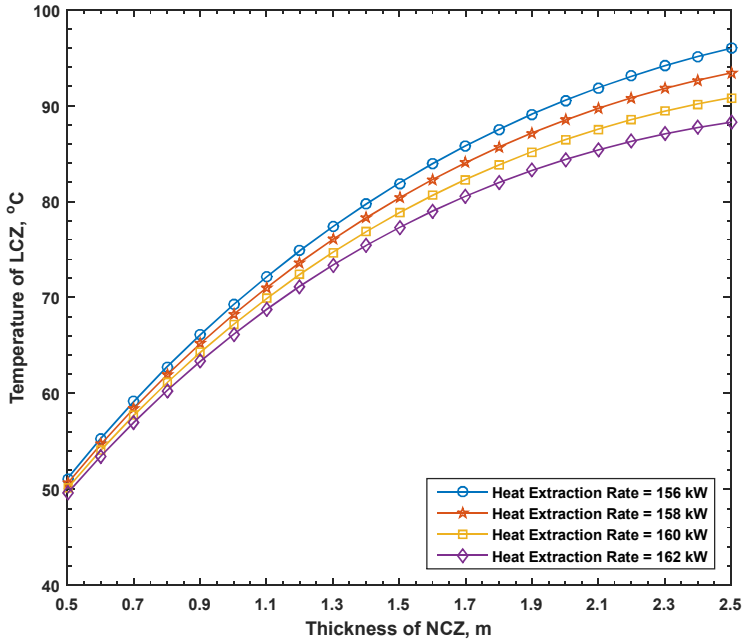

Figure 4. Effect of *NCZ* thickness and heat extraction rate on the *LCZ* temperature.

On the other hand, the temperature of the *LCZ* decreases with the heat extraction rate while the absorption chiller must be provided with temperature values close to 80 °C to work efficiently [16]. Referring to Figure 4, if the thickness of the *NCZ* is fixed at a certain

value, 1.5 m for example, the extraction rate should be controlled so as not to exceed 158 kW to ensure that the temperature does not fall below 80 °C.

4.1.3. Effect of Annual Average Global Radiation and Annual Average Ambient Temperature on the Performance of the Pond

The effect of annual average global radiation on the performance of the pond is shown in Figure 5. Four values are chosen for *NCZ* thickness: 0.5, 1, 1.5, and 2 m.

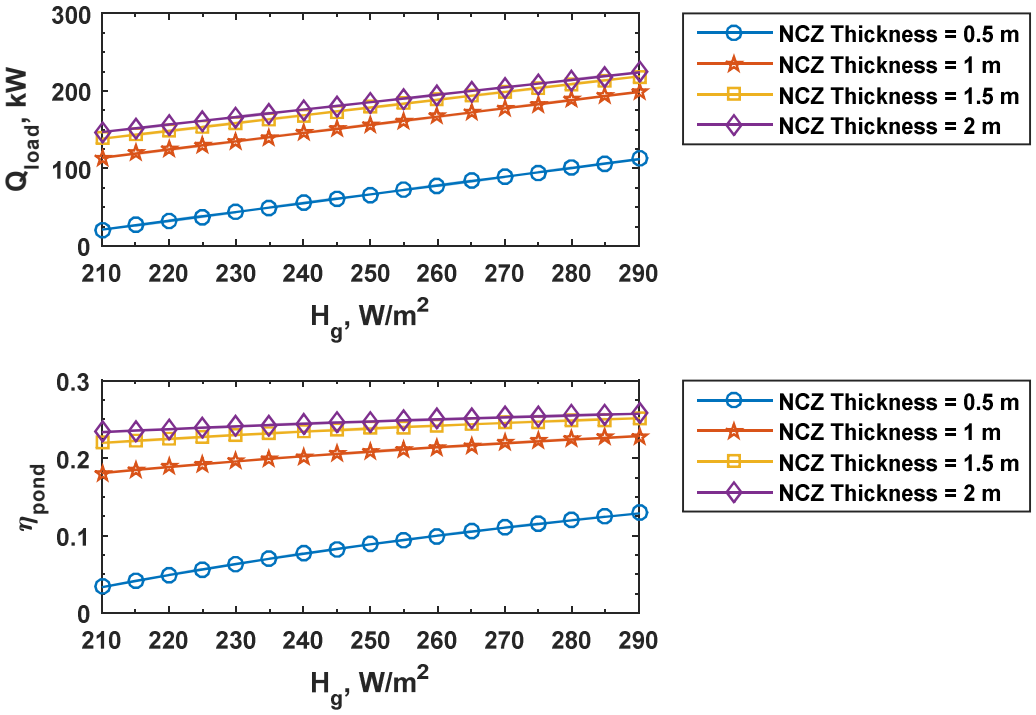

Figure 5. Effect of annual average global radiation on the performance of the pond.

If the *NCZ* thickness and the *LCZ* temperature are considered to be 1.5 m and 80 °C, respectively, the output of the pond increases linearly with average global solar radiation while the efficiency increases at a slightly decreasing rate. The rate of improvement of extraction rate and efficiency decreases as *NCZ* thickness increases. The improvement becomes almost insignificant when the thickness exceeds 1.5 m. In correspondence of 1.5 m thickness and *LCZ* temperature of 80 °C, as the annual global radiation increases from 210 to 290 W/m^2, the available annual average extraction rate increases from 138.4 kW to 218.8 kW, while the annual average efficiency increases from 0.2197 to 0.2515. The percentage increases are 58.1% and 14.5%, respectively.

The effect of annual average ambient temperature on the performance of the pond is shown in Figure 6.

As can be observed, both the output and efficiency of the pond increase linearly with the average ambient temperature. This is expected as the thermal losses decrease with the decrease in the difference between *LCZ* and ambient temperatures. Additionally, in this case, the effect of *NCZ* thickness is significant at low values of thickness and almost disappears when the thickness exceeds 1.5 m. As can be shown in the figure, at an *NCZ* thickness of 1.5 m and *LCZ* temperature of 80 °C, as the average ambient temperature rises from 18 to 34 °C, the annual average extraction rate available increases from 150.7 to 171.4 kW while the annual average collection efficiency increases from 0.2184 to 0.2485. Therefore, the resulting improvements are 13.7% and 13.8%, respectively.

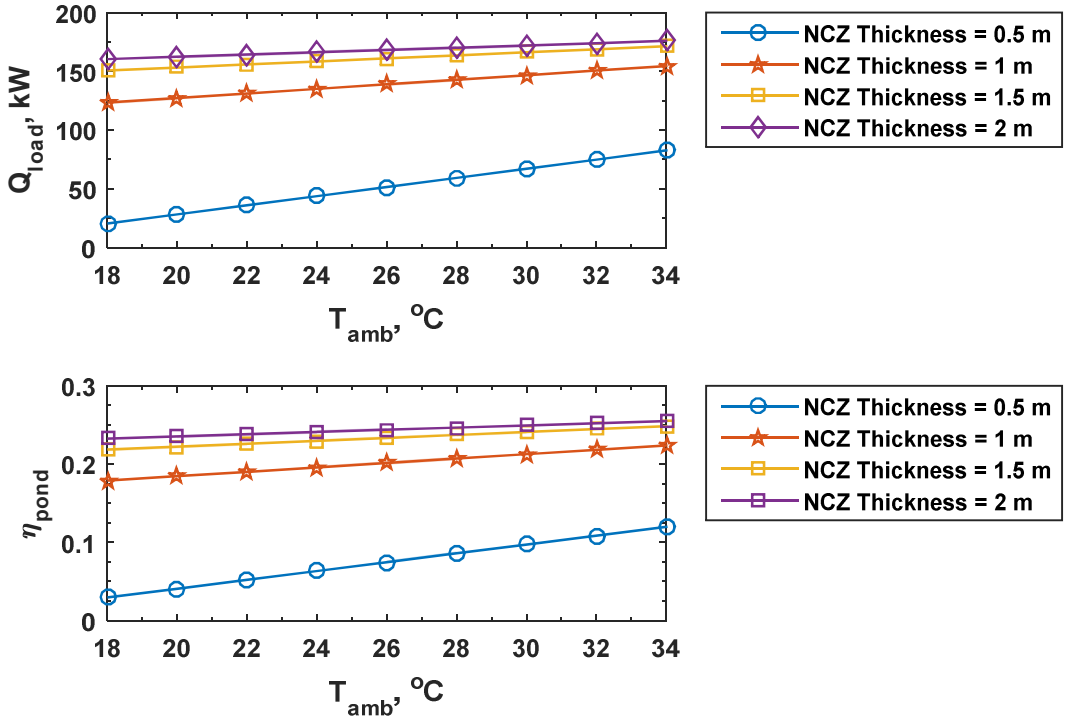

Figure 6. Effect of annual average ambient temperature on the performance of the pond.

4.1.4. Effect of Average Global Radiation and Ambient Temperature on the *LCZ* Temperature

According to the solar atlas of Jordan, the average daily global irradiance changes from one location to another and can reach up to 7 kWh/m^2, corresponding to the solar intensity of 291.7 W/m^2. The same can be said for the average ambient temperature, which can exceed 30 °C. In Jordan, 8 months have an annual average ambient temperature that exceeds 25 °C. The annual average ambient temperature from March to November is equal to 27 °C [21,32,34].

If the extraction rate is kept at 158.5 kW and the thickness of the *NCZ* is 1.5 m, it can be shown in Figure 7 that if the average global radiation rises from 210 to 240 W/m^2, the temperature of *LCZ* will increase from 64.49 to 87.74 °C. Additionally, if the average ambient temperature rises from 18 to 34 °C, the temperature of the *LCZ* will increase from 73.99 to 89.99 °C.

In some applications, such as space air conditioning, the cooling load is required only during the summer months, in which the global radiation and the ambient temperature are higher than the annual average values. Based on that, the thickness of the pond can be optimized according to more favorable conditions. As can be observed in Figure 7, fixing the reference temperature supplying the absorption chiller at 80 °C, if the annual average global radiation increases from 222 to 230 W/m^2, the thickness required to achieve the same output decreases from 2 to 1.5 m. This can be observed by drawing a horizontal line corresponding to the temperature of 80 °C and noting the points of intersection. The same effect can be observed for the annual average ambient temperature. If it increases from 18 to 26 °C, the required *NCZ* thickness decreases from 2 to 1.5 m.

Another thing that can be observed from the same figure is that the effect of *NCZ* thickness on the *LCZ* temperature decreases with increasing thickness. This confirms once again that there is a limit to the thickness of the *NCZ* beyond which the effect on the temperature of the *LCZ* disappears.

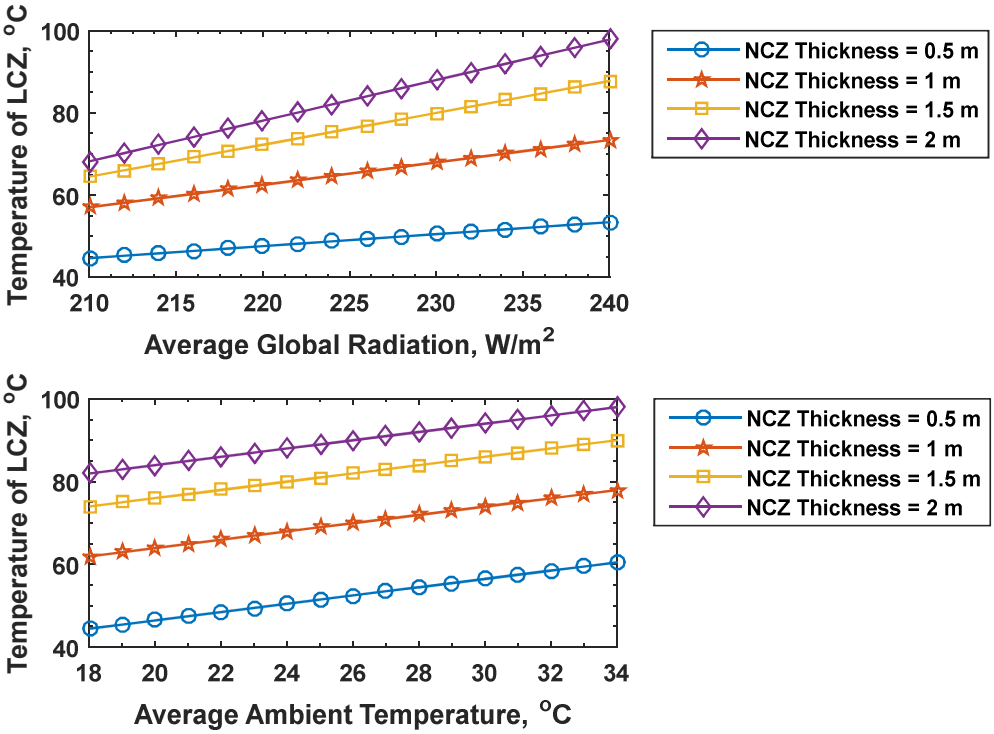

Figure 7. Effect of average global radiation and average ambient temperature on the *LCZ* temperature.

4.2. Absorption Subsystem

The main parameters that affect the performance of the chiller are the operating temperatures of the four main components that make it up, T_g, T_c, T_a and T_e. The ranges of these temperatures are identified by using a *P-T-X* diagram to avoid crystallization and by the operating temperature limits at which the performance parameters approach zero [35,36].

4.2.1. Optimization of the Performance of Absorption Chiller with Respect to Generator and Evaporator Temperatures

Figure 8 shows the effects of generator and evaporator temperatures on chiller performance. As the generator temperature rises, the *COP* increases to an optimum value of approximately 0.799 at a temperature close to 85 °C. The cooling capacity shows the same trend and reaches a value of 126.6 kW. After exceeding the maximum value, a slight drop is observed and this can be attributed to an increase in entropy generation in the generator.

It can be observed that assuming a cooling water temperature of 24 °C, corresponding to the annual average temperature in the Dead Sea area, and assuming the fluid in the condenser and absorber to be at 11 degrees higher than this value or 35 °C, as the generator temperature change from 75 to 95 °C, there is a slight improvement in the coefficient of performance from 0.781 to 0.795. It is also noted that the cooling capacity shows a slight improvement from 123.7 to 126 kW. This means that once the generator temperature rises above the value of 75 °C, its effect on the chiller performance becomes insignificant. Therefore, it is important to keep the temperature of the heat carrier from the pond above this value. This range is typical for solar ponds with optimized thickness and controlled extraction rate. If, for example, the reference temperature was fixed at 80 °C and the *LCZ* temperature was controlled to be maintained around this value during long operating periods, there is a guarantee that the chiller will continue to operate at high efficiency throughout the operating period.

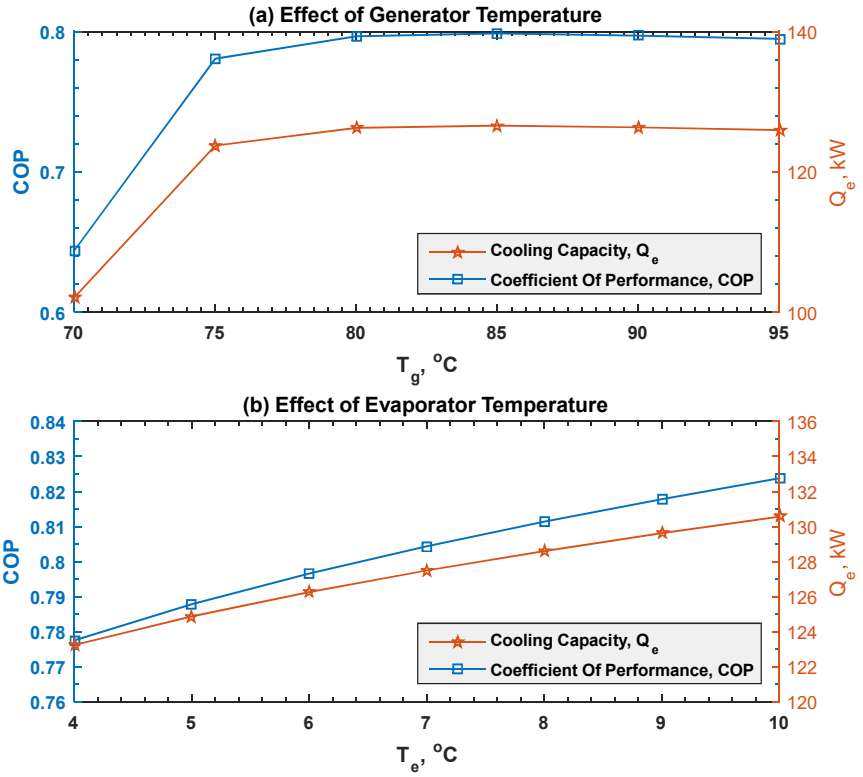

Figure 8. Generator and evaporator temperatures effects on chiller performance.

Both the *COP* and cooling capacity are increasing steadily with evaporator temperature with a slight decrease rate. As the evaporator temperature increases from 4 to 10 °C, the coefficient of performance increases from 0.778 to 0.824 with an improvement of 5.95%. The rated value of the evaporator temperature depends on the application load and the lower limit is subject to the freezing of water in the evaporator. In the case under consideration, the value 6 °C was considered. If the climatic conditions of the Dead Sea region are considered, with an annual average of cooling water considered to be equal to 24 °C and assuming that the temperature of the condenser and absorber is 11 degrees more than that, or equal to 35 °C, it is noted that at a reference temperature of 80 °C, the coefficient of performance is equal to 0.797 and the cooling capacity is equal to 126.3 kW.

4.2.2. Optimization of the Performance of the Absorption Subsystem with Respect to the Cooling Temperature

Figure 9 shows the effects of condenser and absorber temperatures on chiller performance. Both the *COP* and $\dot{Q}_e$ decrease with increasing cooling temperature. It is observed that there is a slight decrease in the beginning followed by a rapid drop when the condenser and absorber temperature exceeds 40 °C.

This finding shows that the performance of the chiller is slightly affected as long as the condenser and absorber temperatures are below this value. The effects of T_c and T_a are evaluated at T_g = 80 °C, T_e = 6 °C, and ε_{SHE} = 0.8. Therefore, it can be said that the proposed system provides an effective solution to this problem, as the condenser and absorber are cooled by drawing water from the *UCZ* of the pond. The temperature of the *UCZ* is usually close to ambient in winter but lower in summer due to evaporation from the pond surface [12]. With lower humidity in the air, evaporation is greater and the evaporative cooling effect is more effective [37]. Therefore, the proposed solution provides a guarantee of not reaching the limit that leads to the deterioration of the performance of the chiller and also eliminates the need to use a cooling tower.

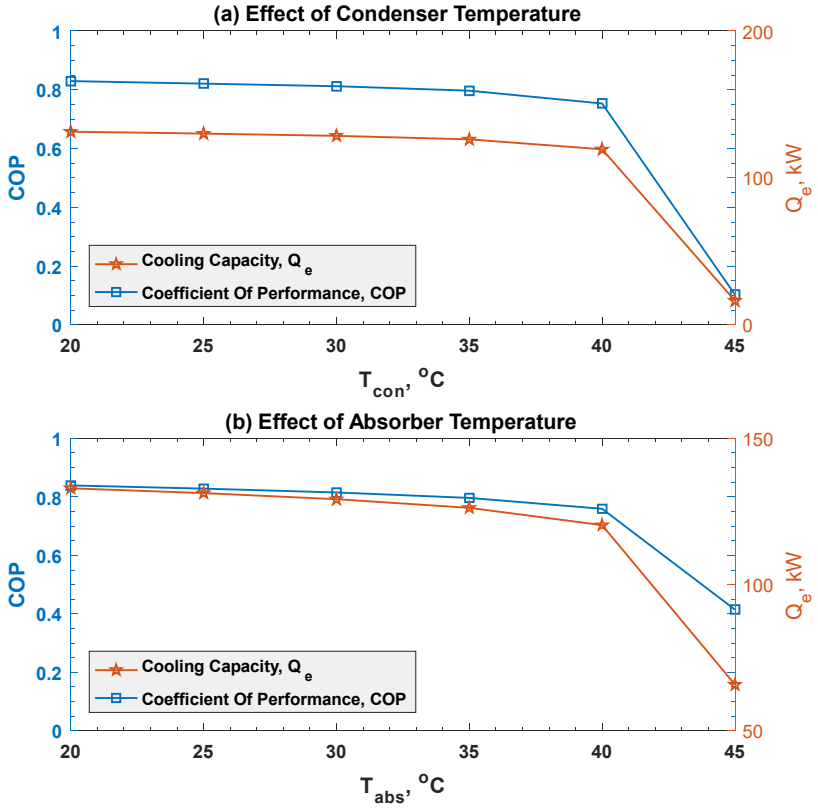

Figure 9. Condenser and absorber temperatures effects on chiller performance.

4.3. Performance of Overall System

4.3.1. Effect of Hot Source Temperature on the Performance of the Overall System

The hot source temperature is the temperature of the fluid leaving the *LCZ* of the pond and moving to the generator. The performances of the solar pond subsystem, the absorption subsystem, and the overall system in the function of the hot source temperature are shown in Figure 10. It can be observed that with the increase in temperature, the efficiency of the solar pond decreases while the *COP* of the absorption chiller increases rapidly up to a certain optimum value and then starts declining gradually. Accordingly, the overall system will take a maximum and optimum value which is equal to 0.187 and takes place at a hot source temperature of 75 °C.

By observing the figure, an important result is the relative stability of the *COP* of the overall system over a wide range of hot source temperatures changing from 70 to 90 °C. In fact, the lowest value of 0.16 takes place at 70 °C and the highest value of 0.187 takes place at 75 °C, which means a change of 16.6% during a temperature range of 25 degrees. This high level of stability allows the system to track the changes in the influencing parameters without having a significant impact on the coefficient of performance. In correspondence to the reference hot source temperature of 80 °C, the efficiency of the pond is 0.23, the *COP* of the chiller is 0.797 and the *COP* of the overall system is 0.183.

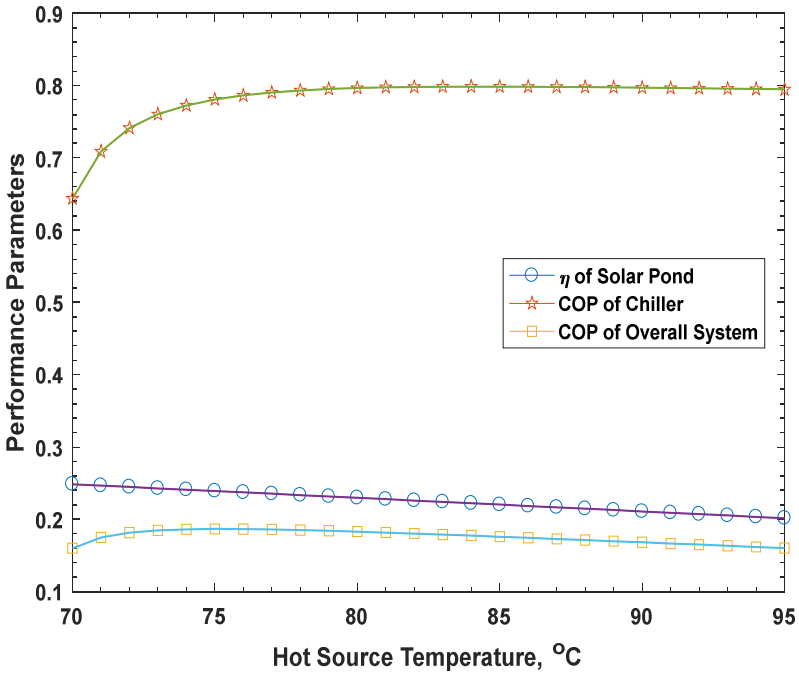

Figure 10. Effect of hot source temperature on the performance of the overall system.

4.3.2. Effect of Environmental Conditions on the Performance of the Overall System

Once the thickness of *NCZ* is fixed, the extraction temperature is controlled by controlling the heat extraction rate from the pond. Other parameters that affect the performance of the overall system are the average global solar radiation and average ambient temperature. The effects of these parameters are shown in Figures 11 and 12. It can be observed in Figure 11 that, due to an increase in global solar radiation, the coefficient of performance of the overall system increases at a slightly decreasing rate while the cooling capacity increases almost linearly. In addition, the changes in the coefficient of performance and cooling capacity are more relevant at higher values of hot source temperature as the curves become closer to each other.

This can be explained by noticing that the decrease in the performance of the pond becomes more dominant than the increase in the performance of the chiller at higher values of hot source temperature. At the reference temperature of 80 °C, as the global radiation increased from 210 W/m^2 to 290 W/m^2, the coefficient of performance of the overall system increased from 0.175 to 0.20 corresponding to a 14.5% improvement. On the other hand, the cooling capacity increased from 110.2 to 174.3 kW, corresponding to a 58.17% improvement.

The effects of average ambient temperature on the *COP* of the overall system and the cooling capacity are shown in Figure 12. It can be observed that both the *COP* of the overall system and the cooling capacity increase slightly until they reach a certain value and then start decreasing. At a certain value of ambient temperature, a sharp drop can be observed. This can be explained by noting that there are two opposite effects of increasing the ambient temperature, one of which leads to an increase in the efficiency of the pond, and the second of which reduces the efficiency of the chiller. This reduction is due to the subsequent increase in the temperature of the *UCZ* and thus to the increase in the cooling temperature of the condenser and absorber. Therefore, it can be concluded that the first effect is slightly dominant at low values of average ambient temperature, while the second effect prevails significantly at high values. Another thing that can be observed is the effect of hot source temperature. Some hot source temperature values were selected in the range in which the chiller has high *COP*. At low values of ambient temperature, the system performs better when hot source temperatures are low while the opposite occurs at high values. From this result, it is possible to derive a control method linking both temperatures, the hot source temperature and the ambient temperature, so that if the ambient temperature increases,

the temperature of the hot source can be increased so as to avoid an unwanted decline in system performance.

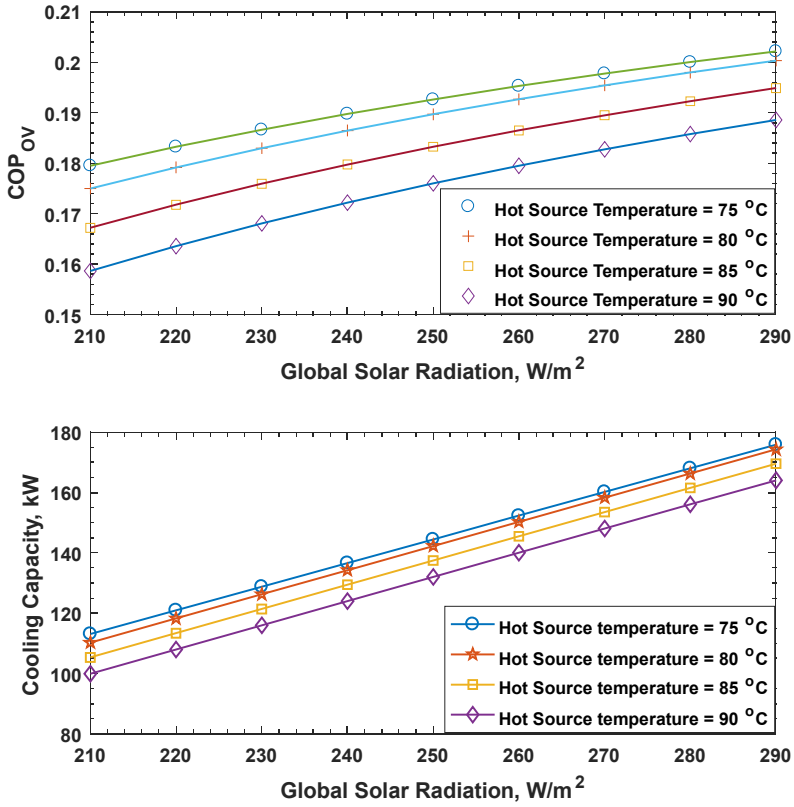

Figure 11. Effect of average global solar radiation on the performance of the overall system.

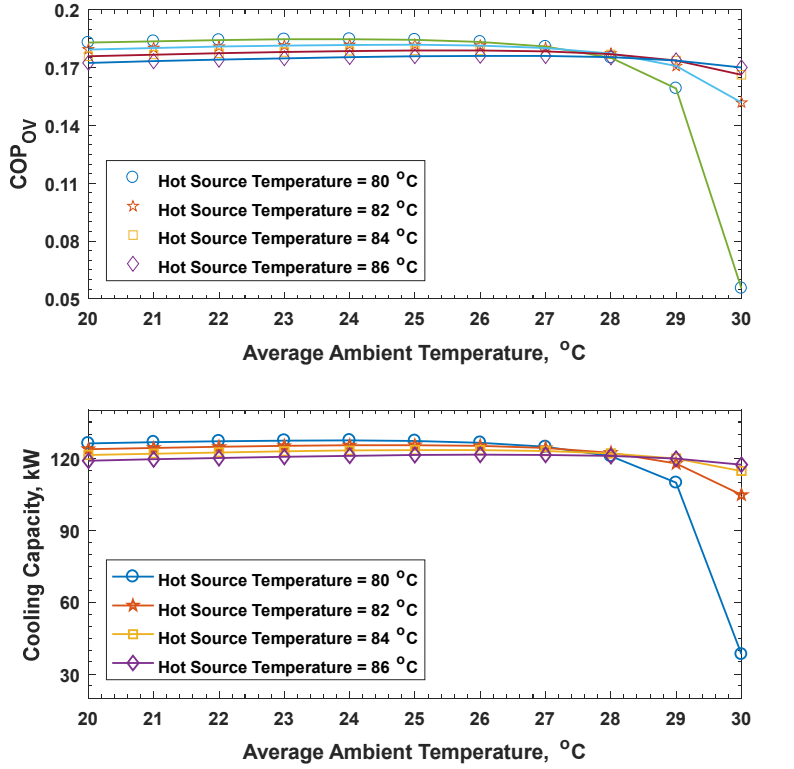

Figure 12. Effect of average ambient temperature on the performance of the overall system.

4.3.3. Effect of Evaporator Temperature on the Performance of the Overall System

The effect of evaporator temperature on the coefficient of performance of the overall system is shown in Figure 13. The *COP* of the overall system increases with evaporator temperature and, as expected, this effect is similar to the effect on the *COP* of the chiller, as this temperature has no direct effect on the performance of the solar pond.

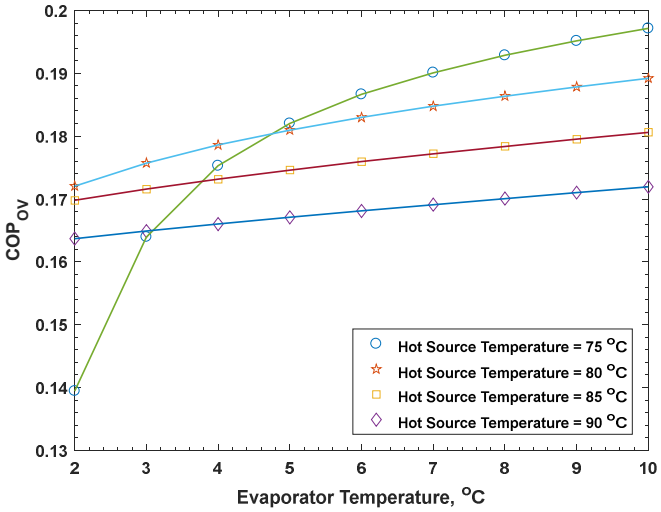

Figure 13. Effect of evaporator temperature on the *COP* of the overall system.

On the other hand, it is noted that there is an inverse relationship between the rate of increase in the coefficient of performance and the temperature of the hot source and because of this result, points of intersection between the curves appeared. The points of intersection help in controlling the hot source temperature according to the values taken by the temperature of the evaporator, so that the effort is made to improve the coefficient of performance. Once the thickness of the *NCZ* is fixed, to improve the performance of the overall system, the extraction temperature must be controlled taking into account the heat extraction rate, the intensity of solar radiation, ambient temperature and the temperature of the evaporator. Condenser and absorber cooling temperatures are affected by environmental conditions near the surface of the pond. With proper system control, these parameters can be monitored and the actual performance can be detected and optimized.

4.4. Model Validation

The model of the solar pond can be validated by comparison with experimental systems. The results presented by many experimental models showed that the temperature of the *LCZ* is almost stabilized after a warm-up period [12,38]. There are also a number of theoretically validated models that led to the same conclusion [5,26].

Regarding the numerical results, unfortunately, there are no results that give the annual average values to be compared with predicted values. The available results give the average monthly values over a period of one year or more, so these values were used to calculate the average annual values. Three experimental models with different locations and specifications are considered: (1) El Paso solar pond [12,38]; (2) Solvay Minerales solar pond [1]; and (3) Kuwait City solar pond [26]. The respective specifications are given in Table 1.

Table 1. Specification of El Paso, Solvay Minerales and Kuwait City solar ponds.

Parameters	El Paso	Solvay Minerales	Kuwait City
Area	3000 m^2	500 m^2	8 m^2
UCZ thickness	0.7 m	0.2 m	0.2 m
NCZ thickness	1.2 m	1.4 m	0.4 m
LCZ thickness	1.35 m	0.6 m	0.3 m
Average global radiation	5.7 kWh/m^2·d	4.87 kWh/m^2·d	5.4 kWh/m^2·d
Average ambient temperature	17.3 °C	11.7 °C	25.9 °C
Latitude	31.773088	37.05	29.3759
Longitude	−106.505730	−3.75	47.9774
Average *LCZ* temperature	81.1 °C	73 °C	80.5 °C
UCZ temperature	15.7 °C	20 °C	16.3 °C

The model was run using the specifications of the three ponds and a comparison between the experimental and theoretical results is shown in Table 2.

Table 2. Comparison between experimental and predicted results of solar ponds.

Solar Pond	Experimental Average *LCZ* Temperature	Predicted Average *LCZ* Temperature
El Paso	81.1 °C	84.1 °C
Solvay Minerales	73 °C	73 °C
Kuwait City	80.5 °C	81.8 °C

Based on these results, it can be concluded that there is an acceptable agreement between the experimental and calculated results since the deviations in the model results do not exceed the value of 3.6%. The differences can be attributed to the assumptions considered when the model was introduced, such as assuming that the *UCZ* and *LCZ* are fully mixed layers with uniform properties, neglecting the heat losses from the bottom and the sides and assuming the *UCZ* to have a temperature equal to the ambient temperature.

The absorption chiller model was validated by comparing the theoretical results with available experimental results in the literature. The same parameters for both theoretical and experimental results were used, T_e = 5 °C, T_c = 30 °C, T_a = 30 °C and ε_{SHE} = 0.4. The effects of the generator and evaporator temperatures on the *COP* of the chiller are shown in Figure 14. As shown, the results of the current study are in good agreement with the experimental results presented by Aphornratana et al. [36]. The percentage of mean absolute error between the theoretical and experimental results for *COP* change with generator temperature was 1.78% and with evaporator temperature was 0.58%.

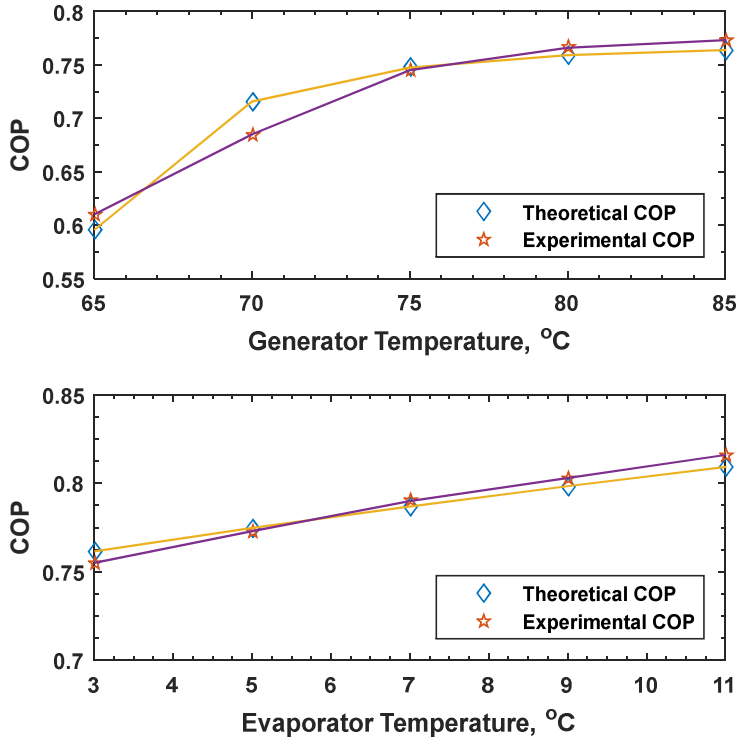

Figure 14. Validation of absorption chiller model.

5. Conclusions and Recommendations

In this study, a salinity gradient solar pond driving an absorption chiller was analyzed as an alternative to conventional electric-powered cooling systems. Solar ponds are characterized by high storage capacity with low cost and steady load availability and can supply thermal power at temperatures that exceed the limit required to activate solar absorption units. Because of the work described here, the following conclusions can be drawn:

- Coupling a solar pond with an absorption chiller results in a system that is reliable and sustainable and ideally suited to hot areas such as Jordan and countries with similar weather. This coupling is useful in facing two difficulties arising from characteristics of solar radiation, its low energy density and its irregularity;
- Careful selection of the rate of heat extraction rate from the pond helps in maintaining the temperature of the pond storage layer in the range of 75–95 °C, which is suitable for efficient chiller operation over long periods of time;
- By choosing an appropriate place to implement the proposed system, such as the Dead Sea area in Jordan, which has favorable climatic conditions, a 3000 m^2 surface area solar pond coupled with an absorption chiller was optimized and was able to supply a heat flow rate of 158.5 kW with an efficiency of 0.23. The chiller was able to produce a cooling capacity of 126.3 kW with a coefficient of performance of 0.797; therefore, the overall system coefficient of performance was equal to 0.183;
- If the temperature of *LCZ* and the thickness of *NCZ* are fixed, the heat extraction rate and the efficiency of the pond increase with the annual average global solar radiation and with the annual average ambient temperature;
- If the heat extraction rate and the thickness of the *NCZ* are fixed, the temperature of *LCZ* increases with the annual average global solar radiation and with the annual average ambient temperature;
- If the heat extraction rate is fixed, there is a certain thickness at which the *LCZ* temperature takes a maximum value;
- Both the *COP* and $\dot{Q}_e$ of the absorption unit increase with hot source temperature to reach optimum values and then show a gradual decrease and both are characterized by high stability over a wide range of temperature variations between 75 and 95 °C;

- Both the *COP* and $\dot{Q}_e$ of the absorption unit are slightly affected as long as the condenser and absorber temperatures are below 40 °C;
- The proposed method of cooling the condenser and the absorber helps to avoid reaching the point of deterioration in the performance of the chiller and eliminates the need for use of a cooling tower;
- With the increase in the hot source temperature, the efficiency of the solar pond decreases while the *COP* of the absorption chiller increases so that the *COP* of the overall system takes a maximum and optimum value at a certain temperature;
- The *COP* of the overall system has a high level of stability over a wide range of hot source temperatures and takes a maximum value of 0.187 at a temperature of 75 °C;
- Both the *COP* and cooling capacity of the overall system increase with average global radiation while the increase in average ambient temperature has two opposite effects, one increases the efficiency of the pond and the other reduces the performance of the chiller;
- At low values of ambient temperature, the system performs better at lower hot source temperatures while the opposite happens at higher values of ambient temperature;
- There is an inverse relationship between the rate of increase in the coefficient of performance of the overall system with evaporator temperature and hot source temperature, such as both values can be controlled simultaneously to increase the performance of the system;
- The prediction of the model showed good agreement with the experimental results as the deviations of model results for the solar pond were within 3.6% and for the absorption chiller were within 1.78%;
- In light of the results that were reached, it is recommended to conduct further research that includes the implementation of an experimental system to carefully evaluate the performance and feasibility of the proposed system in real working conditions and to analyze the effects of the key parameters that govern the overall efficiency. More research is needed on the technical and economic optimization of pond and chiller sizes depending on real conditions, such as changes in temperature and solar radiation. Finally, it is recommended to initiate performance and economic studies to determine the potential for use of the system in specific applications, such as residential heating and cooling systems, and to identify the steps to be taken towards developing the system from the research phase to the commercial phase.

Funding: This research received no external funding.

Data Availability Statement: The author confirms that the data supporting the findings of this study are available within the article.

Conflicts of Interest: The author declares no conflict of interest.

Nomenclature

A,B,C	constants
Aj	constants related to light absorption
Ap	pond surface area (m^2)
c_1, c_2	constants of integration
COP	coefficient of performance
COP_{ov}	overall system performance
h	specific enthalpy (kJ/kg)
$\hat{H}_g$	annual average global solar radiation (Wm^{-2})
k	fluid thermal conductivity ($Wm^{-1}K^{-1}$)
K_j, K'_j	constants related to light absorption (m^{-1})
l_1	upper Convective Zone thickness (m)
l_2	non-Convective Zone thickness (m)

L	pond total depth (m)
$\dot{m}$	mass flow rate (kg/s)
n_1, n_2	refraction indices of first and second mediums
Q_{load}	annual average heat extracted rate (W)
$\dot{Q}$	heat flow rate (kW)
T	temperature (°C)
T_I	annual average temperature of *UCZ* (°C)
T_{II}	annual average temperature of *NCZ* (°C)
T_{III}	annual average temperature of *LCZ* (°C)
x	depth of water (m), mass fraction of lithium bromide, (kg LiBr/kg solution)
Greek Letters	
δ	declination angle
ε_{HE}	heat exchanger effectiveness
$\hat{\eta}$	annual average pond efficiency
θ_1	effective angle of incidence for annual average values
θ_2	refraction angle
λ	solar radiation wavelength (μm)
ρ_b	beam radiation reflectivity
δ	declination angle
τ_a	transmissivity based on absorption
τ_r	transmissivity based on reflection
φ	latitude
ω	hour angle, frequency (Hz)
Subscripts	
a	absorber
amb	ambient
c	condenser
e	evaporator
g	generator
i	state point or index i = 1, 2, 3 . . .
r	refrigerant
ss	strong solution
ws	weak solution
Abbreviations	
A	absorber
C	condenser
E	evaporator
G	generator
HE	solution heat exchanger
LCZ	lower convective zone
NCZ	non-convective zone
UCZ	upper convective zone
SGSP	salinity gradient solar pond

References

1. Alcaraz, A.; Montalà, M.; Cortinaa, J.L.; Akbarzadeh, A.; Aladjem, C.; Farran, A.; Valderran, A. Design, construction, and operation of the first industrial salinity-gradient solar pond in Europe: An efficiency analysis perspective. *Sol. Energy* **2018**, *164*, 316–326. [CrossRef]
2. Amigo, J.; Suárez, F. Ground heat storage beneath salt-gradient solar ponds under constant heat demand. *Energy* **2018**, *144*, 657–668. [CrossRef]
3. Saleh, A.; Qudeiri, J.A.; Al-Nimr, M.A. Performance investigation of a salt gradient solar pond coupled with desalination facility near the Dead Sea. *Energy* **2011**, *36*, 922–931. [CrossRef]
4. Weinberger, H. The physics of the solar pond. *Sol. Energ* **1964**, *8*, 45–46. [CrossRef]
5. Rabl, A.; Neilsen, C.E. Solar ponds for space heating. *Sol. Energ* **1975**, *17*, 1–12. [CrossRef]

6. Kooi, C.F. The steady state salt gradient solar pond. *Sol. Energ* **1979**, *2*, 37–45. [CrossRef]
7. Verma, S.; Das, R. Effect of ground heat extraction on stability and thermal performance of solar ponds considering imperfect heat transfer. *Sol. Energy* **2020**, *198*, 596–604. [CrossRef]
8. Hawlader, M.N.A.; Brinkworth, B.J. An analysis of the non-convecting solar pond. *Sol. Energy* **1981**, *27*, 195–204. [CrossRef]
9. Tian, D.; Qu, Z.G.; Zhang, J.F.; Ren, Q.L. Enhancement of solar pond stability performance using an external magnetic field. *Energy Convers. Manag.* **2021**, *243*, 114427. [CrossRef]
10. Boudhiaf, R.; Ben Moussa, A.; Baccar, M. A Two-Dimensional Numerical Study of Hydrodynamic, Heat and Mass Transfer and Stability in a Salt Gradient Solar Pond. *Energies* **2012**, *5*, 3986–4007. [CrossRef]
11. Anagnostopoulos, A.; Sebastia-Saez, D.; Campbell, A.N.; Arellano-Garcia, H. Finite element modelling of the thermal performance of salinity gradient solar ponds. *Energy* **2020**, *203*, 117861. [CrossRef]
12. Lu, H.; Walton, J.C.; Swift, A.H.P. Desalination coupled with salinity-gradient solar ponds. *Desalination* **2001**, *136*, 13–23. [CrossRef]
13. Duffie, J.A.; Beckman, W.A.; Blair, N. *Solar Engineering of Thermal Processes, Photovoltaics and Wind*, 5th ed.; John Wiley & Sons, Inc.: Hoboken, NJ, USA, 2020.
14. Ullah, K.R.; Saidur, R.; Ping, H.W.; Akikur, R.K.; Shuvo, N.H. A review of solar thermal refrigeration and cooling methods. *Renew. Sustain. Energy Rev.* **2013**, *24*, 499–513. [CrossRef]
15. Fathi, R.; Gumimi, C.; Ouaskit, S. An irreversible thermodynamic model for solar absorption refrigerator. *Renew. Energy* **2004**, *29*, 1349–1365. [CrossRef]
16. Saleh, A.; Mosa, M. Optimization study of a single-effect water–lithium bromide absorption refrigeration system powered by flat-plate collector in hot regions. *Energy Convers. Manag.* **2014**, *87*, 29–36. [CrossRef]
17. Ren, J.; Qian, Q.; Yao, Z.; Gan, N.; Zhang, Y. Thermodynamic Evaluation of LiCl-H_2O and LiBr-H_2O Absorption Refrigeration Systems Based on a Novel Model and Algorithm. *Energies* **2019**, *12*, 3037. [CrossRef]
18. Abid, M.; Khan, M.S.; Tahir, T.A.H.; Malik, M.N.; Ali, H.M.; Cheok, Q. Thermodynamic analysis and comparison of different absorption cycles driven by evacuated tube solar collector utilizing hybrid nanofluids. *Energy Convers. Manag.* **2021**, *246*, 114673. [CrossRef]
19. Saleh, A.; Al-Nimr, M.A. A novel vacuum wastewater treatment plant integrated with a solar absorption system. *Int. J. Energy Res.* **2020**, *44*, 1685–1697. [CrossRef]
20. Al-Falahi, A.; Alobaid, F.; Epple, E. Design and Thermo-Economic Comparisons of an Absorption Air Conditioning System Based on Parabolic Trough and Evacuated Tube Solar Collectors. *Energies* **2020**, *13*, 3198. [CrossRef]
21. Alrwashdeh, S.S.; Alsaraireh, F.M.; Saraireh, M.A. Solar radiation map of Jordan governorates. *Int. J. Eng. Technol.* **2018**, *7*, 1664–1667. [CrossRef]
22. Tsilingiris, P.T. Large scale solar cooling design using salt gradient solar ponds. *Renew. Energy* **1991**, *1*, 309–314. [CrossRef]
23. Tsilingiris, P.T. The absorption chiller in large scale solar pond cooling design with condenser heat rejection in the upper convecting zone. *Sol. Energy* **1992**, *49L*, 19–27. [CrossRef]
24. Kanan, S.; Dewsbury, J.; Lane-Serff, G.F. Simulation of Solar Air-Conditioning System with Salinity Gradient Solar Pond. *Energy Procedia* **2015**, *79*, 746–751. [CrossRef]
25. Salata, F.; Tarsitano, A.; Golasi, I.; Vollaro, E.L.; Coppi, M.; Vollaro, A.L. Application of Absorption Systems Powered by Solar Ponds in Warm Climates for the Air Conditioning in Residential Buildings. *Energies* **2016**, *9*, 821. [CrossRef]
26. Chakrabartya, G.S.; Wankhedea, U.S.; Shelkea, R.S.; Gohilc, T.B. Investigation of temperature development in salinity gradient solar pond using a transient model of heat transfer. *Sol. Energy* **2020**, *202*, 32–44. [CrossRef]
27. Kasaeian, A.; Sharifi, S.; Yan, W. Novel achievements in the development of solar ponds: A review. *Sol. Energy* **2018**, *174*, 189–206. [CrossRef]
28. Chevallier, J.; Isern, L.; Almandoz, F.K.; Chalk, C.; Nicholls, J.R. Modelling evaporation in electron-beam physical vapour deposition of thermal barrier coatings. *Emergent Mater.* **2021**, *4*, 1499–1513. [CrossRef]
29. Ayou, D.S.; Coronas, A. New Developments and Progress in Absorption Chillers for Solar Cooling Applications. *Appl. Sci.* **2020**, *10*, 4073. [CrossRef]
30. Stocker, W.; Jones, J.W. *Refrigeration and Air Conditioning*; McGraw Hill: Singapore, 1982.
31. ASHRAE. *ASHRAE Handbook of Fundamentals*; ASHRAE: Atlanta, GA, USA, 1985.
32. Climate Conditions in Dead Sea. Available online: http://hikersbay.com/climate-conditions/israel/deadsea/climate-conditions-in-dead-sea.html?lang=en#weather-temperature-months (accessed on 5 October 2022).
33. Hull, J.; Nielsen, C.E.; Golding, P. *Salinity Gradient Solar Ponds*; CRC Press: Boca Raton, FL, USA, 1989.
34. Worlddata.info. Available online: https://www.worlddata.info/asia/jordan/climate.php (accessed on 5 October 2022).
35. Kaynakli, O.; Kilic, M. Theoretical study on the effect of operating conditions on performance of absorption refrigeration system. *Energy Convers. Manag.* **2007**, *48*, 599–607. [CrossRef]
36. Aphornratana, S.; Sriveerakul, T. Experimental studies of a single-effect absorption refrigerator using aqueous lithium-bromide: Effect operating condition to system performance. *Exp. Therm. Fluid Sci.* **2007**, *32*, 658–669. [CrossRef]

37. Çengel, Y.A.; Ghajar, A.J. *Heat and Mass Transfer: Fundamentals & Applications*, 5th ed.; McGraw-Hill Education: New York, NY, USA, 2015; pp. 882–883.
38. Leblanc, J.; Akbarzadeh, A.; Andrews, J.; Lu, H.; Golding, P. Heat extraction methods from salinity-gradient solar ponds and introduction of a novel system of heat extraction for improved efficiency. *Sol. Energy* **2011**, *85*, 3103–3142. [CrossRef]